Transport and Deposition of Particles in Turbulent and Laminar Flow

Abhijit Guha

Aerospace Engineering Department, University of Bristol, Bristol BS8 1TR, United Kingdom; email: A.Guha@bristol.ac.uk

Key Words

turbulent, diffusion, turbophoresis, thermophoresis, inertial impaction, Lagrangian tracking, Eulerian advection-diffusion

Abstract

This article reviews the physical processes responsible for the transport and deposition of particles and their theoretical modeling. Both laminar and turbulent processes are considered, emphasizing the physical understanding of the various transport mechanisms. State-of-the-art computational methods for determining particle motion and deposition are discussed, including stochastic Lagrangian particle tracking and a unified Eulerian advection-diffusion approach. The theory presented includes Brownian and turbulent diffusion, turbophoresis, thermophoresis, inertial impaction, gravitational settling, electrical forces, and the effects of surface roughness and particle interception. The article describes two example applications: the deposition of particles in the human respiratory tract and deposition in gas and steam turbines.

1. INTRODUCTION

In this article I discuss the physical processes by which solid particles (or liquid droplets) suspended in a fluid are transported to and deposited on solid walls. Measuring, predicting, and understanding the deposition rate are both scientifically interesting and important in engineering (in a variety of areas of mechanical engineering, chemical engineering, environmental science, and medicine); consequently, these have been the subject of a very large number of studies. After presenting experimental facts, theoretical developments, and computational procedures on deposition, I discuss two examples: the deposition of drugs and harmful substances in the respiratory tract (in medical science and engineering) and the deposition of particles and droplets in gas and steam turbines (in mechanical engineering). Similar physical processes take place in the atmospheric dispersal of pollutants and the determination of indoor air quality (in environmental science), the transport and sedimentation of various substances in rivers (in civil engineering), the fouling of process and heat transfer equipments (in mechanical engineering), and the transport of chemical aerosols (in chemical engineering), along with many other examples. This review emphasizes the physical understanding of transport and deposition and provides sufficient details for the reader to undertake state-of-the-art computations of deposition both in the Lagrangian (including stochastic) and Eulerian frameworks.

In this review we consider only dilute mixtures (i.e., when the volume fraction of the dispersed phase is low). The particles or droplets therefore are assumed not to interact with each other and to exhibit one-way coupling (i.e., the particle motion depends on the fluid flow field but not vice versa). Many practical situations conform to such a description. The theory presented covers both laminar and turbulent flow of the fluid. Natural convection may also contribute to setting up the fluid flow field. Some of the particle transport mechanisms are also operative in a static fluid (e.g., gravitational settling, Brownian diffusion, transport due to electrostatic forces).

There are two common approaches for deposition calculations: Eulerian and Lagrangian. As a result of the one-way coupling assumption, it is possible, for the Eulerian computational scheme, to compute the fluid flow field first, followed by a separate solution of the equations for the particles. However, the equations for the particle motion presented in this article can also be solved simultaneously with the equations for fluid motion, if one so wishes. The Lagrangian schemes involve trajectory calculations typically for a large number of particles moving in a fluid turbulence field that is generated by various methods, ranging from simple ones to direct numerical simulation (DNS) of Navier-Stokes equations. The implication of the one-way coupling in this context is that one can track each particle independently from other particles; hence it is possible to perform parallel computations.

Unless otherwise stated, in this review x is the main direction of fluid flow, and y is perpendicular to a solid surface (on which deposition occurs). The particle properties are denoted by the subscript p, and fluid properties are either given without subscript (for readability) or by the subscript f (where it enhances clarity).

2. GENERAL EXPERIMENTAL CHARACTERISTICS OF DEPOSITION AND FICK'S LAW OF DIFFUSION

Usually the results of deposition experiments or calculations are presented as curves of nondimensional deposition velocity versus nondimensional particle relaxation time. The deposition velocity, V_{dep}, is the particle mass transfer rate on the wall, $\mathcal{J}_{wall}$, normalized by the mean or bulk density of particles (mass of particles per unit volume), $\rho_{p,m}$, in the flow:

$$V_{dep} = \mathcal{J}_{wall}/\rho_{p,m}. \qquad (1)$$

The particle relaxation time, τ, is a measure of particle inertia and denotes the time scale with which any slip velocity between the particles and the fluid is equilibrated. As demonstrated below, τ depends, among other things, on the particle radius; hence the abscissa of the usual deposition curves represents increasing particle radius. V_{dep} and τ are made dimensionless with the aid of the fluid friction velocity u_*: $V_{dep}^+ = V_{dep}/u_*$, $\tau^+ = \tau u_*^2/\nu$, where ν is the kinematic viscosity of the fluid ($\nu = \mu/\rho$).

Many previous studies give experimental measurements of the deposition velocity (Friedlander & Johnstone 1957, Liu & Agarwal 1974, McCoy & Hanratty 1977, Wells & Chamberlain 1967). Although there is considerable scatter, these data illustrate the basic characteristics shown in **Figure 1**. The results fall into three distinct categories: (*a*) At first, as τ^+ increases, the deposition velocity decreases. This is the so-called turbulent diffusion regime, in which a turbulent version of Fick's law of diffusion (see below) applies. (*b*) The striking feature of the next zone, the so-called eddy diffusion-impaction regime, is that the deposition velocity increases by three to four orders of magnitude. (*c*) The third regime of deposition, usually termed the particle inertia moderated regime, results in an eventual decrease in the deposition velocity for large particle sizes. The borders between the three regimes are not sharp, as one effect gradually merges into another, and depend on flow conditions.
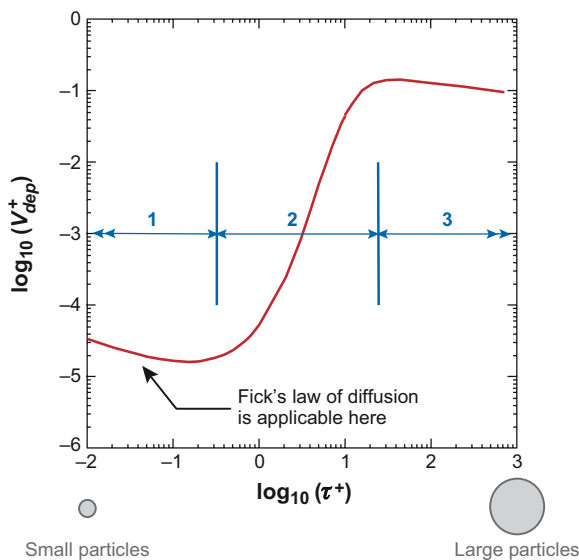

Figure 1

A typical variation in measured deposition rate with particle relaxation time in fully developed vertical pipe flow. Regime 1, turbulent diffusion; regime 2, turbulent diffusion-eddy impaction; regime 3, particle inertia moderated.

2.1. Molecular and Turbulent Diffusion

Most mass-transfer textbooks (e.g., Kay & Nedderman 1988) show that one can calculate the flux of small particles in a turbulent boundary layer by integrating a modified Fick's law of diffusion,

$$J = -(D_B + D_t)\frac{d\rho_p}{dy}, \qquad (2)$$

where D_B is the Brownian diffusivity; D_t is the turbulent diffusivity, which varies with position; y is the perpendicular distance from the wall; and $\frac{d\rho_p}{dy}$ is the gradient of particle partial density (same as concentration gradient). D_B is given by the Einstein equation incorporating Cunningham's (1910) correction ($C_C = 1 + 2.7\text{Kn}$) for rarefied gas effects,

$$D_B = \left(\frac{kT}{6\pi\mu r}\right)C_C, \qquad (3)$$

where k is the Boltzmann constant, T is the absolute temperature, and Kn is the Knudsen number defined by $\text{Kn} = l/2r$, where l is the mean free path of the surrounding gas and r is the radius of a particle. Another semiempirical form for the Cunningham factor, $C_C = 1 + \text{Kn}[a + b\exp(-c/\text{Kn})]$, is also widely used: Davies (1945) gave the values of the constants as $a = 2.514$, $b = 0.8$, and $c = 0.55$. Slightly different values for these constants are sometimes used in the literature. Equation 3 shows that D_B decreases with increasing r. Equation 2 therefore predicts that the mass flux of particles and deposition velocity decrease continuously with increasing particle size. **Figure 1** shows a more complex behavior, and Fick's law does not give a complete description. We describe in the following sections both Lagrangian and Eulerian computational methods to illustrate what happens in the second and third regimes of deposition velocity.

3. PARTICLE MOTION AND VARIOUS FORCES

This section describes a few common forces that affect particle motion. The magnitudes of various forces are expressed as those per unit mass of the particle (because both Eulerian and Lagrangian schemes are conveniently expressed in terms of particle acceleration). The following equations contain vector quantities; hence magnitudes and directions need to be accounted for properly. The effects of virtual mass and the Basset history term (Maxey & Riley 1983) are usually not included in deposition studies—both these terms are small when the ratio of particle material density and fluid density is large ($\rho_p^0/\rho \gg 1$), a condition generally satisfied for the motion of solid particles or liquid droplets in a gas.

3.1. Aerodynamic Drag F_D

A particle moving in a fluid experiences a drag force. The drag force is always present, and it acts as a mechanism by which a particle tries to catch up with the changing velocities of the surrounding fluid (for discussions on the physical aspects of relaxation phenomena, see Becker 1970; Guha 1995, 2007). The drag force F_D

(per unit mass of the particle) may generally be expressed as

$$F_D = \frac{V_f - V_p}{\tau}, \tag{4}$$

where V_f and V_p are fluid and particle velocities, respectively. The equation applies to instantaneous as well as time-mean values. For spherical particles with small slip velocity ($\Delta V = V_f - V_p$), the magnitude of the drag force is given by the Stokes result, $F_D = 6\pi r\mu|\Delta V|/m$, where m is the mass of an individual particle ($m = \frac{4}{3}\pi r^3 \rho_p^0$, where ρ_p^0 is the density of pure particulate material). Inserting this result into Equation 4, one finds that in the Stokes drag regime τ is given by

$$\tau = 2\rho_p^0 r^2/9\mu. \tag{5a}$$

The curves for the variation of V_{dep}^+ versus τ^+ are plotted with this definition of the relaxation time. However, in the numerical calculations, one needs to correct the relaxation time to account for the slip velocity for large particles and the rarefied gas effects for very small particles. The rarefied gas effects can be modeled by the Cunningham correction factor C_C as used in Equation 3, whereas the effects of a large slip Reynolds number are modeled by incorporating an empirical particle drag coefficient, C_D. The general expression for the inertial relaxation time τ_I is then given by

$$\tau_I = \tau \frac{24}{\mathrm{Re}C_D} C_C, \tag{5b}$$

where Re is the slip Reynolds number defined as $\mathrm{Re} = 2r|\Delta V|/\nu$, and C_D is a function of Re. Morsi & Alexander (1972) give an empirical equation that is widely used: $C_D = a_1 + a_2/\mathrm{Re} + a_3/\mathrm{Re}^2$, where the values of a_1, a_2, and a_3 are provided in several piecewise ranges of Re. Another much used equation is $C_D = (24/\mathrm{Re})(1 + 0.15\mathrm{Re}^{0.687})$; Clift et al. (1978) attribute this equation to Schiller and Nauman, dating back to 1933.

The aerodynamic drag for nonspherical particles is usually expressed as an empirical correction to the drag of equivalent spheres by introducing suitable shape factors. Various geometric shape factors for a particle of an arbitrary shape are proposed by combining two of the four quantities: volume, surface area, projected area, and projected perimeter. For example, a widely used volumetric shape factor is calculated as volume/(4 × projected area/π)$^{3/2}$. Theoretical and experimental values of the drag are more readily available for regular nonspherical shapes (e.g., spheroidal, cylindrical) than for arbitrary shapes, and these values are given by Clift et al. (1978). Different orientations and the possible rotation of nonspherical particles add to the complexity.

Sometimes the concept of an aerodynamic diameter (d_{ae}) is used, which is the diameter of a unit density sphere (usually taken as 1 g cm^{-3}) that has the same gravitational settling speed as the particle in question (aerodynamic drag is therefore the same at the terminal speed). The aerodynamic diameter is given by $d_{ae} = d_V\sqrt{\rho_p^0/S_D}$, where d_V is the diameter of an equivalent spherical particle that has the same volume as the nonspherical particle in question, and S_D is the dynamic shape correction factor. Hinds (1999) gives values for S_D for common geometric shapes and particle types.

3.2. Inertial Impaction

If the magnitude and direction of the fluid velocity (mean velocity in the context of turbulent flow) change rapidly, significant velocity slip may develop (as shown in Equation 4), particularly for larger particles. When the fluid time-mean streamlines are curved, particles may not be able to follow them as a result of inertia, and the deviated particle pathlines may make them collide with nearby solid walls and get deposited, which is known as inertial impaction. This may be an important mechanism, for example, for the highly curved blades in steam and gas turbines or for the complex flow passages with rapid turning in the nasopharyngeal region of the human respiratory tract or in the branching bronchial tree. Inertial impaction may be relevant for either laminar or turbulent flow.

3.3. Gravitational Force F_G

A particle in a gravitational field experiences a force (weight) in the direction of the gravitational acceleration g. The particle also experiences a force in the opposite direction (buoyancy), which, according to the Archimedes principle, is equal to the weight of the displaced fluid. Hence, the net gravitational force (per unit mass of particle), F_G, is given by

$$F_G = \left(1 - \frac{\rho}{\rho_p^0}\right)g. \tag{6}$$

In situations in which gravity and aerodynamic forces are balanced, a particle acquires a terminal speed known as the gravitational settling speed, V_{gs}. One can determine the magnitude of the gravitational settling speed from Equations 4 and 6: $V_{gs} = (1 - \rho/\rho_p^0)g\tau_I$. In noninertial reference frames, centrifugal forces may give rise to similar body force effects like gravity.

3.4. Shear-Induced Lift Force F_S

Saffman (1965, 1968) provided an expression for the shear-induced lift force, which (per unit mass and in the y direction) is

$$F_{Sy} = 1.542 \frac{\rho}{\rho_p^0} \nu \frac{1}{r} \sqrt{\frac{1}{\nu} \left| \frac{d\bar{V}_{fx}}{dy} \right|} \left(\bar{V}_{fx} - \bar{V}_{px}\right). \tag{7}$$

Calculations show that the effect of F_S is usually to enhance deposition velocity. The majority of deposition calculations reported in the literature make use of the Saffman expression for the lift force. However, Saffman originally derived his result for an unbounded shear flow. For deposition calculations, one should use modified expressions for the lift force that include the effects of the proximity of a wall and finite Reynolds numbers. The sign of the Saffman lift force in a particular direction depends on the sign of the slip velocity in the perpendicular direction. Guha (1997, appendix B) discusses a subtle interaction between F_S, gravity, and particle convective velocity toward a wall in vertical flow.

3.5. Thermophoretic Force F_{Therm}

The thermophoretic force depends on the presence of a temperature gradient:

$$F_{Therm} = -(\eta/m)\nabla \ln T. \qquad (8)$$

Talbot et al. (1980) give an equation for the thermophoretic force coefficient, η:

$$\eta = \frac{2.34(6\pi\mu\nu r)(\lambda_r + 4.36\text{Kn})}{(1 + 6.84\text{Kn})(1 + 8.72\text{Kn} + 2\lambda_r)},$$

where λ_r is the ratio of the thermal conductivity of the fluid, λ, and that of the particles, λ_p ($\lambda_r = \lambda/\lambda_p$). Numerical calculations given below show that the thermophoretic force may be significant for smaller particles even in the presence of a modest temperature gradient. In cooled gas turbines, the blade may be cooler than the gas by several hundred degrees Kelvin; the thermal gradient is large; consequently thermophoresis strongly influences the motion of particles in the relevant size range.

3.6. Electrical Forces F_E

A charged aerosol is subjected to electrical forces. If there is an externally applied electric field of strength E and the total charge carried by a particle is q, then the Coulomb force due to the imposed field is qE. A charged aerosol near a solid wall also experiences an electrostatic force owing to induced charges on the wall (mirror charging). The easiest way to find the force is the method of images (Nadler et al. 2003). If the wall is conducting, then it is an equipotential line, and one can find the electrostatic force on a particle at distance y from the wall by placing an opposite charge (image) at $-y$. The electrostatic force due to mirror charging is, in this case, of an attractive nature (i.e., acts toward the wall assisting deposition), and one can calculate its magnitude per unit mass of the particle using Coulomb's law. The total electrical force (per unit mass of a particle) in the y direction is then given by

$$F_{Ey} = \frac{qE}{m} - \frac{3q^2}{64\pi^2\varepsilon_0\rho_p^0 r^3 y^2}, \qquad (9)$$

where ε_0 is the electric permittivity of vacuum (or air). Hesketh (1977) gives an expression for the maximum charging of a particle q_{max}: $q_{max} = 2000 \times (1.6 \times 10^{-19})(r/10^{-6})^2$ Coulomb. To make a parametric investigation of the effects of mirror charging on particle motion, we express $q = \xi q_{max}$. There are other terms (such as dielectrophoretic force, dipole-dipole interaction, interaction due to neighboring particles) that are usually small and are not considered here.

Davies (1966) and Soo (1990) present other aspects of particle dynamics. Crowe (1982) has given a review of the various computational fluid dynamics (CFD) techniques used for two-phase flows.

4. LAGRANGIAN PARTICLE TRACKING CALCULATIONS

A large number of studies have adopted the approach of particle tracking in a Lagrangian framework. For example, Kallio & Reeks (1989) calculated the deposition

of particles in a simulated turbulent fluid field; Ounis et al. (1993) and Brooke et al. (1994) computed the motion of particles for which the fluid motion was determined by DNS of the Navier-Stokes equations; Wang & Squires (1996) solved the fluid velocity field using large eddy simulation; and Fichman et al.'s (1988) and Fan & Ahmadi's (1993) calculations were based on the sublayer approach originally proposed by Cleaver & Yates (1975).

In the particle tracking methods, the momentum equation for the particle is written and then integrated with respect to time along the particle pathline. Typically the motion of a very large number of particles is solved, and from this one can construct statistically meaningful ensemble average quantities. The particle momentum equation and position equation in the i direction can be written on the basis of the discussions in Section 3:

$$\frac{dV_{pi}}{dt} = \frac{V_{fi} - V_{pi}}{\tau_I} + F_{Gi} + F_{Si} + F_{Therm,i} + F_{Ei} + B_i, \tag{10}$$

$$\frac{dx_i}{dt} = V_{pi}. \tag{11}$$

Equations 10 and 11 can be numerically integrated together, giving the new position and velocity at the end of each computational time step. It is straightforward to include other forces not considered here in Equation 10.

The first and last terms in the right-hand side of Equation 10 deserve special mention. If one wants to calculate the impact of fluid turbulence on the particle motion, one must use the instantaneous fluid velocity V_f in the first term. If one uses the time-mean value $\bar{V}_f$ in the first term, no matter what sophisticated turbulent calculation method was used in determining it, proper turbulent diffusion and dispersion characteristics of particles are not captured. The average particle motion calculated by first determining the time-mean fluid velocity and then using Lagrangian tracking through this steady fluid flow field is not the same as first using Lagrangian tracking through a fluctuating fluid flow field and then averaging. Of course, if time-mean $\bar{V}_f$ is used, some particle dispersion and deposition may still be predicted if other mechanisms such as inertial impaction (see Section 3.2) or gravitational settling (Section 3.3) are present, as they would be in a laminar flow. Under certain combinations of flow geometry and particle size, these other mechanisms can even be the dominant factors (but one needs to be aware of these considerations, particularly when using CFD packages to perform Lagrangian particle tracking with time-mean $\bar{V}_f$). The fluctuating turbulent field may also alter the steady-state values of other forces in Equation 10, such as F_S, but such effects are considered small and usually are not included in reported studies. The last term in Equation 10 represents the Brownian force on a particle and must be included especially for small particles (see regime 1 in **Figure 1**).

The attraction of the Lagrangian tracking method is obvious, and the form of Equation 10 is general and direct. The coding of the computer program is relatively simple (as compared with the coding of an Eulerian method). The interactions of particles with the solid boundary (e.g., rebounding) can also be modeled in a simple manner. A polydispersed droplet population, even when a change in particle size is

involved, can be accommodated easily. When the particle inertia is very large and the fluid flow field has significant streamline curvature (such that inertial impaction and/or gravitational settling is the dominant mechanism), then a picture of the particle velocity field and deposition can be built from the Lagrangian tracking of a reasonably small number of particles through the time-mean fluid flow field—such calculations can be relatively inexpensive. Hence, often in the literature one finds mixed Eulerian-Lagrangian calculations in which the mean fluid field in complex three-dimensional geometry is calculated by Eulerian methods, and then Lagrangian calculations are performed on particles. Most commercial CFD codes have this facility. However, if calculation of the particle concentration field is also necessary (e.g., Marchioli & Soldati 2002) in addition to the particle velocity field, then Lagrangian calculations face challenges and can be computationally expensive. Moreover, when particle motion is significantly influenced by fluid turbulence, then Lagrangian calculations with fluctuating fluid velocity are needed (the fluid field being determined by Reynolds-averaged Navier-Stokes, large eddy simulation, or DNS). Such tracking calculations are typically performed for a large number of particles (may be 10^4, 10^5, or many more) for statistically meaningful results, and the computational time step needed is small (particularly for small particles for which Brownian diffusion may also need to be included); hence stochastic Lagrangian calculations are computationally intensive and expensive. The method can thus be a good research tool for understanding the flow physics, but it is unlikely to become a practical method for engineering calculations or be used as a design tool.

4.1. Stochastic Eddy Interaction Models

The instantaneous turbulent fluid velocity may be computed directly by a DNS approach. Often, instead a Monte Carlo simulation (also known as random walk modeling in this context) is performed. In this approach, a particle's stochastic trajectory is modeled as a succession of interactions with turbulent eddies. The time-mean fluid velocity $\bar{V}_f$ is calculated by a suitable turbulent computational method (e.g., the $k - \varepsilon$ model). A simulated fluctuating velocity field is then superposed to calculate the instantaneous fluid velocity ($V_f = \bar{V}_f + V_f'$). A fluid eddy is assigned a fluctuating velocity V_f', which is assumed to stay constant during the lifetime of the eddy t_e. As a particle encounters an eddy on its pathline, Equations 10 and 11 are integrated together to calculate the particle velocity and position at the end of the particle residence time t_r. Small particles usually stay within the same eddy during the eddy's lifetime (then $t_r = t_e$); particles with large inertia may leave the eddy before the eddy decays (in this case, $t_r < t_e$). Once the particle has left the eddy or the eddy lifetime is over, the particle encounters a new eddy at its current location, and the integration of Equations 10 and 11 is repeated in the same manner. The calculation for a particle is continued until the particle is captured by a wall (deposition has then taken place) or goes out of the computational space. The calculation procedure is repeated for many particles.

The differences between the various reported schemes are mainly in how the velocity scale, length scale, and eddy lifetime are generated and randomized. An adopted

scheme should preserve the dispersion characteristics of the original turbulent flow and needs to be validated for this purpose. The method used for calculating the eddy lifetime and eddy length scale determines the Lagrangian and Eulerian autocorrelation, respectively.

Usually these stochastic models calculate the eddy velocity as $V_f' = N_G v_{rms}$, where v_{rms} is the root mean square (rms) of the fluid fluctuating velocity in the relevant direction, and N_G is a random number drawn from a Gaussian probability density distribution of zero mean and unity standard deviation. Another probability density function other than the Gaussian can also be used. If a constant eddy life is used in the simulation, then it should be chosen such that $t_e = 2T_L$, where T_L is the fluid Lagrangian integral time scale, to preserve the long-term dispersion characteristics; random time steps should be used to produce a smooth Lagrangian autocorrelation function (Wang & Stock 1992). Similarly, if a constant eddy length scale (l_e) is used, then it should be chosen such that $l_e = 2L_E$, where L_E is the Eulerian integral length scale (Graham & James 1996). For (solid) particles with finite inertia, the Lagrangian integral time scale for the particle lies between the Lagrangian and Eulerian integral time scales for the fluid.

Gosman & Ioannides (1983) used a $k - \varepsilon$ method for calculating the time-mean fluid velocity field, assumed isotropic fluctuating velocities ($v_{rms,i} = \sqrt{2k/3}$), and calculated the eddy length scale from $l_e = C_\mu^{0.5} k^{1.5} / \varepsilon$ and eddy time scale from $t_e = l_e / |V_f'|$. Hutchinson et al. (1971) used a constant t_e. Shuen et al. (1983) used the same model as Gosman & Ioannides (1983) except they used $t_e = l_e / (\sqrt{2k/3})$. Kallio & Reeks (1989) simulated the turbulent fluid velocity field using empirical curve fittings for the time-mean x velocity $\bar{V}_{f,x}$, rms y fluctuations $v_{rms,y}$, and Lagrangian time scale T_L, all as functions of the wall coordinate y^+. The particle residence time was taken to be always equal to the eddy lifetime ($t_r = t_e$); hence they need not specify the eddy length scale (l_e). The eddy time scale (t_e) was calculated by randomizing the Lagrangian integral time scale T_L from an exponential probability density distribution. Berlemont et al. (1990) provided another approach for stochastic Lagrangian calculation. This method uses a correlation matrix in the random process to explicitly specify any shape of the Lagrangian correlation function.

Kallio & Reeks's (1989) study is important in terms of deposition calculations because (despite its inability to capture regime 1 in **Figure 1** as a result of ignoring Brownian movement) it showed that a simple stochastic theory could predict the general behavior of particle deposition in regimes 2 and 3 in **Figure 1**.

4.2. Markov Chain–Type Turbulent Random Walk Models

There are many papers on this approach particularly developed in the context of atmospheric dispersion (Durbin 1980, Luhar & Britter 1989, Sawford 1982, Walklate 1987). Whereas for the stochastic eddy interaction models the Lagrangian velocities are generated through independent random numbers, for the Markov chain–type simulations the velocities are generated through dependent random numbers with one-step memory. For a one-dimensional case, if $x(t)$ and $v_f(t)$ are the position and velocity, respectively, of a fluid particle or a tracer particle, then the evolution of

(v_f, x) is generally described as

$$dv_f = a(x, v_f)\, dt + \sqrt{(C_0 \varepsilon)}\, d\xi, \tag{12a}$$

$$dx = v_f dt, \tag{12b}$$

where $d\xi$ is a random velocity increment of the Wiener process with zero mean and variance dt, C_0 is a universal constant (Monin & Yaglom 1975), and ε is the mean rate of dissipation of turbulent kinetic energy. The function a is determined by solving a Fokker-Planck equation to satisfy the well-mixed criterion (Thomson 1987), which ensures that a globally uniform source of tracer is not unmixed by the turbulent motions. For the homogeneous, isotropic, stationary case, $a = -v_f/T_L$ and $C_0 \varepsilon = 2 v_{rms}^2 / T_L$, and Equation 12a becomes the basic Langevin equation. It is usually stated that dt should be less than $0.1 T_L$, so that the effect of the size of computational time step does not significantly affect the Lagrangian velocity correlation. Application of this type of random walk model can be complex in strongly inhomogeneous and anisotropic turbulent flow, in multidimensional dispersion problems, and when particle inertia is significant.

4.3. Calculation of the Brownian Force B_i

One can adopt a molecular dynamics approach to calculate Brownian movement. However, in the context of the discussion on the stochastic simulation of turbulence in the previous two sections above, one could either alter the expression for the displacement in the Markov chain process (Borgas & Sawford 1996) or add a force (e.g., Ounis et al. 1993) in the eddy interaction model. In the Markov chain approach, the form of Equation 12a remains the same, but Equation 12b is replaced by $dx = v_f dt + \sqrt{2 D_B} d\xi'$, where $d\xi'$ is a random number representing white noise, and the Brownian diffusion coefficient D_B is given by Equation 3.

In the eddy interaction model, the Brownian force (per unit mass of particle) in each direction is specified as a Gaussian white noise: $B_i = (N_{Gi}/m)\sqrt{(2 k^2 T_f^2)/(D_B \Delta t)}$, where Δt is the computational time step, and N_{Gi} is a Gaussian random number with zero mean.

5. EULERIAN PARTICLE TRANSPORT CALCULATIONS

All practical CFD computations for a single-phase fluid in complex geometries are performed in the Eulerian framework. Hence, it is profitable to solve the particle equations in the same way for easy integration with the established CFD codes for the primary fluid. The Eulerian-Eulerian calculations are computationally efficient (compared with stochastic Lagrangian tracking calculations) and hence are necessary for engineering calculations and as a design tool. However, turbulence closure problems have to be tackled. There are also challenges in implementing physically correct treatment at solid boundaries, including particle rebounding. Crossing trajectories, discontinuities in concentration, and polydispersed particle cloud with temporal change in size of an individual particle (e.g., due to condensation or evaporation;

see Guha 1994, 1995, 1998a; Guha & Young 1991) further complicate the matter.

Historically, it was Eulerian modeling that was first applied to calculate particle deposition in the second regime (regime 2 of **Figure 1**). Starting with Friedlander & Johnstone's (1957) landmark paper, this genre of calculations, variously called stop distance or free flight models, has been used in engineering solutions for a long time. Although these models have contributed strongly to the development of our understanding of deposition, they have fundamental difficulties. Whereas this class of models tried to capture the physics of deposition by solving the particle continuity equation alone, in the past 15 or so years Eulerian computational methods of deposition have been developed that solve both particle continuity and momentum equations (Johansen 1991, Guha 1997, Young & Leeming 1997). These models show that the interaction of particle inertia and the inhomogeneity of fluid turbulent flow field (in the boundary layer close to a solid surface) gives rise to a new mechanism of particle transport called turbophoresis (Caporaloni et al. 1975, Reeks 1983). Turbophoresis (in which particle transport is caused by gradients in fluctuating velocities) is a separate effect and must be treated as such; it cannot be properly reproduced by any tuning of the theoretical model for diffusion (which is driven by the gradients in concentration). Turbophoresis is not a small correction to Fick's law of diffusion; Guha (1997) showed that it is the primary mechanism operative in regimes 2 and 3 of **Figure 1**. Guha (1997) further demonstrated that for large particles, the momentum equation alone can provide nearly accurate estimates of the deposition velocity; the absence of the use of the particle momentum equation in the stop distance models is therefore their major weakness. Theoretical treatments on particle motion in turbulent flow, including kinetic approaches, are given by Reeks (1977, 1991, 1992), Rizk & Elghobashi (1985), Simonin et al. (1993), and Zaichik (1999), among others.

5.1. Stop Distance or Free Flight Models

One of the most used Eulerian calculation methods has been the free flight or stop distance model (e.g., Beal 1970, Davies 1966, Friedlander & Johnstone 1957, Papavergos & Hedley 1984, Wood 1981). These models assume that particles diffuse to within one stop distance, s, from the wall, at which point they make a free flight to the wall. The main difference between different models of this type lies in the prescription of the free flight velocity, v_{ff}. A simple integration of Equation 4 shows that, in nondimensionalized form, $s^+ = (v_{ff}/u_*)\tau^+$. Friedlander & Johnstone (1957) assumed $v_{ff} = 0.9u_*$, a value close to the fluid rms velocity in the outer layer of a turbulent boundary layer. Their model agrees well with experiments in a vertical pipe (in the second regime). Davies (1966) made an apparently more plausible assumption that the free flight velocity is the same as the local rms velocity of the fluid at the point at which the particle starts its free flight, but his calculated deposition velocities were approximately two orders of magnitude lower than the experimental values. Liu & Ilori (1974) improved the prediction of this model by prescribing, rather arbitrarily, a particle diffusivity that was different from the commonly used eddy momentum diffusivity. Beal (1970) gave another variation of the stop distance model.

These models, although significantly contributing to the development of our understanding, are physically not satisfactory. The stop distance models predict a monotonic rise in stopping distance (which may exceed the buffer layer thickness of a turbulent boundary layer for larger particles because $s^+ \sim \tau^+$) and consequently predict a monotonic increase in deposition velocity with increasing τ^+. Experiments, however, show a third regime of deposition, usually termed the particle inertia moderated regime, in which the deposition velocity decreases with a further increase in τ^+ (see **Figure 1**). Stop distance models are not of much use here, and new theories (e.g., Reeks & Skyrme 1976) need to be applied.

Thus, even for the apparently simple case of turbulent deposition in a fully developed pipe flow, a separate theory had to be applied for each deposition regime. Although it is possible, with proper tuning of the models (e.g., by prescribing the free flight velocity), to partially reproduce the experimental results for fully developed pipe flow, the theories cannot be extrapolated to two- or three-dimensional flow situations with any great confidence because of their piecemeal nature and the required empirical tuning. Additionally, when other effects such as thermophoresis or electrostatic interaction are present, the stop distance models would need postulations such as that the deposition velocities due to various mechanisms calculated separately can be simply added (linear superposition).

5.2. A Unified Advection-Diffusion Theory

Guha (1997) has established, by deriving from the fundamental Eulerian conservation equations of mass and momentum for the particles, a unified advection-diffusion theory in which turbophoresis arises naturally. The theory includes molecular and turbulent diffusion, thermophoresis, shear-induced lift force, electrical forces, and gravity. It incorporates the effects of surface-roughness elements and particle interception. The framework is general, and the theory can be integrated efficiently with established multidimensional CFD codes for single-phase flow. The theory reduces to Fick's law of diffusion in the limit of small particles, thus linking Fick's law to a broader scheme of particle transport. The prediction of deposition velocity from this Eulerian theory is at least as accurate as those from the state-of-the-art Lagrangian calculations, including DNS studies, but the Eulerian computation is much faster (and the inclusion of Brownian diffusion is simple).

The new Eulerian theory uses Ramshaw's (1979) approach to model the forces on a particle in a flowing fluid stream, in particular how the Brownian diffusion is modeled (see also Fernandez De La Mora & Rosner 1982). Various flow variables (such as fluid and particle velocity, particle partial density) are decomposed into their mean and fluctuating parts, and then the particle continuity and momentum conservation equations are Reynolds averaged. The resulting equations are then simplified, identifying and retaining the dominant terms, so that clear physical meaning could be ascribed to each term. The equations given in Guha (1997) are general and can, for example, be used to study particle deposition in a developing boundary layer. Here, only the equations for fully developed, vertical flow are discussed to bring out the essential flow physics.

If the flux of particles in the y direction (which is perpendicular to the solid wall) is denoted by J, then the Reynolds averaging of the particle continuity equation for fully developed flow gives

$$\partial J/\partial y = 0,$$

where

$$J = -(D_B + D_t)\frac{\partial \bar{\rho}_p}{\partial y} - D_T \bar{\rho}_p \frac{\partial \ln T}{\partial y} + \bar{\rho}_p \bar{V}_{py}^c, \qquad (13)$$

where D_T is the coefficient of diffusion due to temperature gradient, and $\bar{V}_{py}^c$ is the particle convective velocity in the y direction. Any quantity with an overbar denotes its time-mean value. D_T is given by

$$D_T = D_B(1 + \eta/kT). \qquad (14)$$

Equation 14 shows that the thermal drift has a stressphoretic component and a thermophoretic component (the term containing η). The stressphoretic component arises from the evaluation of ∇p_p, where p_p is the partial pressure of a hypothetical ideal gas consisting of the particle cloud (Ramshaw 1979).

Equation 13 is the generalized equation for particle flux. The particle convective velocity in the y direction, $\bar{V}_{py}^c$, has to be calculated from the particle momentum equation. The Reynolds-averaged particle momentum equations in the y and x directions, slightly simplified and specialized for fully developed vertical flow, are

$$y \text{ momentum:} \quad \bar{V}_{py}^c \frac{\partial \bar{V}_{py}^c}{\partial y} + \frac{\bar{V}_{py}^c}{\tau_I} = -\frac{\partial \overline{V_{py}'^2}}{\partial y} + F_{Sy} + F_{Ey}, \qquad (15a)$$

$$x \text{ momentum:} \quad \bar{V}_{py}^c \frac{\partial \bar{V}_{px}}{\partial y} = \frac{1}{\tau_I}(\bar{V}_{fx} - \bar{V}_{px}) + \left(1 - \rho_f/\rho_p^0\right) g. \qquad (15b)$$

In Equation 15a, $\bar{V}_{py}^c \frac{\partial \bar{V}_{py}^c}{\partial y}$ is the acceleration term, $\frac{\bar{V}_{py}^c}{\tau_I}$ is the steady-state viscous drag (simplified with the assumption $\bar{V}_{fy} = 0$), $-\frac{\partial \overline{V_{py}'^2}}{\partial y}$ is the turbophoresis, F_{Sy} is the shear-induced lift force, and F_{Ey} is the electrical force. Equation 15b represents downward flow; for upward flow, one should replace g with $-g$. Note that the x momentum (Equation 15b) involves both $\bar{V}_{px}$ and $\bar{V}_{py}^c$. The y momentum (Equation 15a) is, however, almost decoupled and depends on $\bar{V}_{px}$ only through the shear-induced lift force, F_{Sy}. A study of Equations 15a and 15b also shows nicely how gravity affects the y-momentum equation through the lift force. The left-hand side of Equation 15b involves $\bar{V}_{py}^c$. As a result of this convective velocity in the y direction, the direction of the lift force may remain unaltered whether the flow is vertically downward or upward.

In the general case, both Equations 15a and 15b must be solved simultaneously. Calculations show that the shear-induced lift force increases the deposition rate, particularly in the eddy diffusion-impaction regime. The effect of the lift force, F_{Sy}, is not considered below. With these provisos, $\bar{V}_{py}^c$ can be calculated from

$$\bar{V}_{py}^c \frac{d}{dy}\left(\bar{V}_{py}^c\right) + \frac{\bar{V}_{py}^c}{\tau_I} = -\frac{d}{dy}\left(\overline{V_{py}'^2}\right) + F_{Ey}. \qquad (15c)$$

The second term on the left-hand side of Equation 15c is the steady-state drag simplified with the assumption $\bar{V}_{fy} = 0$; the full form is $-(\bar{V}_{fy} - \bar{V}_{py}^c)/\tau_I$. The first term

on the right-hand side of Equation 13 is the diffusion due to a gradient in the particle concentration (same as Fick's law given by Equation 2); the second term represents the diffusion due to a temperature gradient; and the third term represents a convective contribution arising owing to particle inertia. Equation 15c relates the particle convective velocity with the gradient in turbulence intensity (turbophoresis) and other external forces. It is chiefly the absence of this convective term in Fick's law that necessitated postulating stop distance or free flight models. From Equation 15c, one can write the expression for turbophoretic velocity ($V_{p,turbo}$) as $V_{p,turbo} = \tau_I [-\frac{d}{dy}(\overline{V_{py}'^2})]$. Importantly, the turbophoretic term depends on the particle rms velocity which may be different from the fluid rms velocity if the particle inertia is large (see Equation 17). When the particles are very small, they effectively follow the fluid eddies, and the two rms velocities are essentially the same. In this limit, $\tau_I \rightarrow 0$, the expression for turbophoretic velocity then shows that $V_{p,turbo} \rightarrow 0$. Turbophoresis is thus negligible for small particles even if there exists a gradient in fluid turbulence intensity. Fick's law is, therefore, an adequate description for the deposition of small particles. As τ_I increases, the turbophoretic term assumes dominance, thereby increasing the deposition rate by a few orders of magnitude. However, as τ_I increases, the particles are less able to follow fluid fluctuations, and the particle rms velocity becomes progressively smaller as compared with the fluid rms velocity. This is one of the factors responsible for the eventual decrease in deposition velocity with increasing particle size when τ_I is very large. The turbophoretic velocity vanishes ($V_{p,turbo} = 0$), for all particles irrespective of the particle inertia, when the flow is either not turbulent or when the turbulence is homogenous [$\partial/\partial y (\overline{V_{fy}'^2}) = 0$]. However, even in laminar flow, Equations 13 and 15 apply and can predict all such effects like Brownian diffusion, thermophoresis, and convective slip velocity due to streamline curvature and external body forces such as gravity or electrical interactions.

For not too large particles, the steady-state drag term (second term on the left-hand side of Equation 15c) almost balances the turbulence term (right-hand side), and the acceleration term (first term on left-hand side) is negligible. The acceleration term assumes importance for large particles and should not be neglected: It is the chief reason why the deposition velocity eventually decreases in the third regime (see **Figure 1**). Neglecting the acceleration term would predict a constant deposition velocity at large τ^+. [Interestingly, such constancy in deposition velocity is characteristic of some of the previous calculations; even Fan & Ahmadi's (1993) Lagrangian calculations show this behavior.]

The unified advection-diffusion theory is logical in finding the combined effects of different particle transport mechanisms, as the appropriate forces are added in the momentum equation, and the combined velocity or flux is calculated directly by solving the continuity and momentum equations. This should be superior to the often-used linear addition of respective velocities, each calculated separately, to determine the combined mass flux.

Fluid and particle root-mean-square velocities. Equations 13–15 would work well if one could find an accurate expression for the particle rms velocity as a function of the wall coordinate. The variation of fluid rms velocity as a function of wall

coordinate can be determined from measurements (Bremhorst & Walker 1973, Finnicum & Hanratty 1985, Kreplin & Eckelmann 1979, Laufer 1954), near-wall modeling work (Chapman & Kuhn 1986), and DNS (Kim et al. 1987). Kallio & Reeks (1989) have given an empirical curve fit for the region $0 < y^+ < 200$ (this equation is quoted below after correcting errors in the original paper):

$$\sqrt{(\overline{V_{fy}'^+})^2} = 0.005 y^{+2}/(1 + 0.002923 y^{+2.128}). \qquad (16)$$

Accurate prediction of fluid rms velocity is important. Other equations with piecewise continuous (and differentiable) curve fits can be used, if deemed appropriate.

It is possible to relate the particle mean square velocity to the fluid mean square velocity through a parameter $\Re$, which is defined as the ratio of the two:

$$\Re = \overline{V_{py}'^2}/\overline{V_{fy}'^2}. \qquad (17)$$

It is difficult to devise a simple but accurate mathematical model for $\Re$, particularly in an inhomogeneous turbulence field. In reality, there should be a memory effect by which the migrating particles tend to retain the turbulence levels of earlier instants. Shin & Lee (2001) give a theoretical constitutive relation for the particle Reynolds normal stress in the presence of a memory effect.

In a practical Eulerian-type calculation, estimates of $\Re$ may have to be made from local turbulence properties. This may not be very accurate, especially because the gradient of fluid turbulence near the wall is very high. In defense of such a simple calculation scheme, however, one may cite that the (not unsuccessful) mixing length theories of fluid turbulence employ similar assumptions. Simple theories of homogeneous, isotropic turbulence (Reeks 1977) predict that, for the particles to be in local equilibrium with the fluid turbulence,

$$\Re = T_L/(\tau_I + T_L), \qquad (18)$$

where T_L is the Lagrangian time scale of fluid turbulence. Binder & Hanratty (1991) and Vames & Hanratty (1988) report some measurements in this area. Binder & Hanratty (1991) provide the following experimental correlation for $\Re$ (their equation 18):

$$\Re = \frac{1}{1 + 0.7(\tau_I/T_L)}. \qquad (19)$$

$\Re$ varies with the wall coordinate because T_L varies. For very small particles $\tau_I \to 0$, and consequently $\Re \to 1$. In other words, very small particles essentially follow fluid turbulence. For large particles, $\tau_I \to \infty$ and $\Re \to 0$. Although $\Re \to 0$, Equation 18 or 19 shows that the product $\tau^+ \Re$, however, remains finite in this limit and becomes independent of τ^+. This is why neglect of the acceleration term in Equations 15 would predict a constant deposition velocity when τ^+ is very large.

It is instructive to plot and study the detailed variations of $\overline{V_{fy}'^2}$ and $\overline{V_{py}'^2}$ with τ^+ for various values of τ_I/T_L because of the importance of such variations in understanding the nature of turbophoresis.

Turbulent diffusivity and eddy viscosity. Theories show that the Schmidt number in homogenous isotropic turbulence in gases is close to 1; i.e., $D_t \approx \varepsilon$ (Pismen & Nir

1978, Reeks 1977). DNS by Brooke et al. (1994) showed that the Schmidt number varied across a pipe from 0.6 to 1.4. In the past, sometimes efforts have been made to stick to Fick's law and (nonphysically) alter the value of particle diffusivity (e.g., Liu & Ilori 1974) to obtain agreement between theoretical and experimental deposition rates. In contrast, the numerical illustrations below show that the particle diffusivity can be approximated by the same value as in homogeneous isotropic turbulence (if a better model is not available) but that a convective particle drift arises in an inhomogenous field by quite a different physical effect—turbophoresis. It is Fick's law itself that needs to be augmented in inhomogenous turbulent flow and when other effects such as body forces are present (Equation 13).

Davies (1966) and Granville (1990), among others, give expressions for the eddy momentum diffusivity ε.

Effects of interception and surface roughness. Guha (1997) gives details on how to account for surface roughness. It is assumed that, on a rough surface, the virtual origin of the velocity profile is shifted by a distance e away from the wall (Grass 1971), where $e = f(k_s)$, k_s being the effective roughness height. The particles are assumed to be captured when they reach the level of effective roughness height, i.e., at a distance b above the origin of the velocity profile, where $b = k_s - e = k_s - f(k_s)$. Grass's (1971) data are sparse, and more measurements (or DNS results) are needed to accurately determine the exact form of $f(k_s)$; when such an expression is available, it can easily be used with the unified advection-diffusion deposition theory. For numerical illustrations, a simple linear relation, $e = 0.55 k_s$, proposed by Wood (1981) is therefore used.

Finally, the effect of interception is accounted for by assuming that a particle is captured when its center is at a distance r away from the effective roughness height, where r is the radius of the particle. The lower limit of the integration domain is taken as $y^+ = y_0^+ = y_0 u_*/\nu$, where y_0 is given by

$$y_0 = b + r. \tag{20}$$

Solution procedure and boundary conditions. If the lift force is included in the study, Equations 13, 15a, and 15b are to be solved simultaneously to determine $\bar{\rho}_p$, $\bar{V}_{px}$, and $\bar{V}_{py}$. The equations are best solved by a time-marching technique. For a simple analysis, Equations 13 and 15c are solved for $\bar{\rho}_p$ and $\bar{V}_{py}$. Equation 15 is nonlinear; it is thus robustly solved by a time-marching technique by introducing a time-derivative term in the equation and then marching forward in time until convergence is obtained, at which point the time-derivative term vanishes, and thus the solution obtained is that of the original equation. If the nonlinear acceleration term is neglected, then a simpler numerical solution of Equation 15c is possible, but the computed values of the deposition velocity will have limitations, as explained above in the discussion following Equation 15c. For fully developed flow, the numerical solution procedure for the continuity equation involving only the y direction is straightforward; recognizing Equation 13 gives $\frac{d}{dy}\{-(D_B + D_t)\frac{d\bar{\rho}_p}{dy} - D_T\bar{\rho}_p\frac{d\ln T}{dy} + \bar{\rho}_p\bar{V}_{py}^c\} = 0$: One writes the equation in discretized finite-difference form at each grid point, and then

Gaussian or Gauss-Jordan elimination may be used to solve values of $\bar{\rho}_p$ at each grid point.

Equation 15c is a first-order differential equation. It can be written in finite-difference form and integrated with one boundary condition. ($\bar{V}_{py}^c = 0$ at the channel centerline or at a sufficient distance away from the wall at which the gradient in turbulence intensity is negligibly small. In a boundary layer type calculation, one could specify the laminar slip velocity at the edge of the boundary layer.) Equation 15c does not depend on particle concentration; hence it can be solved first on its own, and the computed values of $\bar{V}_{py}^c(y)$ can then be used to solve the particle continuity equation. Equation 13 shows that $\bar{\rho}_p$ needs two boundary conditions. These are provided by specifying values of $\bar{\rho}_p$ at the channel centerline (or at a sufficient distance away from the wall) and at the lower boundary y_0 (given by Equation 20).

It is sometimes assumed in mass transfer calculations that the concentration at the lower boundary is zero ($\bar{\rho}_p = 0$, at $y = y_0$). Rigorous derivations based on kinetic theory show that this boundary condition is strictly not true even in the pure diffusion limit of very small particles. In the pure inertial limit of large particles, a more appropriate condition at the lower boundary is $\partial \rho_p / \partial y = 0$. It is found, however, that, in the inertial limit, the effects of such boundary conditions on the magnitude of the calculated deposition velocity are negligible, but the concentration profile close to the wall does depend on the particular boundary condition employed. Moreover, one may need to consider the rebounding of particles from the solid wall and the resuspension of previously deposited particles. For a proper formulation of the boundary condition for the particle concentration at the wall, one would have to resort to kinetic theory. Finding an appropriate boundary condition is one of the challenges of Eulerian modeling.

The particle concentration changes rapidly with distance close to the surface. One therefore needs a nonuniform computational grid to solve the particle continuity equation. The first two grids perpendicular to the solid surface should be taken very close to each other; the grid spacings toward the free stream can then vary according to a suitable geometric progression.

6. EFFECTS OF VARIOUS PARTICLE TRANSPORT MECHANISMS ON OVERALL DEPOSITION RATE

Most experiments and theoretical treatments on particle deposition explore the fully developed vertical flow. Without streamline curvature in time-mean motion (thus eliminating inertial impaction) and with gravitational settling playing a minor role, the effects of molecular and turbulent processes on deposition can be studied more effectively in this configuration. However, Guha's (1997) particle equations automatically describe inertial impaction and gravitational settling when they are present. McCoy & Hanratty's (1977) compiled experimental data show considerable scatter; here only Liu & Agarwal's (1974) data are plotted as this is generally accepted as one of the most dependable data sets and to keep the discussion focused. The experiments were conducted in a glass pipe of internal diameter (D) 1.27 cm; monodispersed, spherical droplets of uranine-tagged olive oil were used (thus the deposition
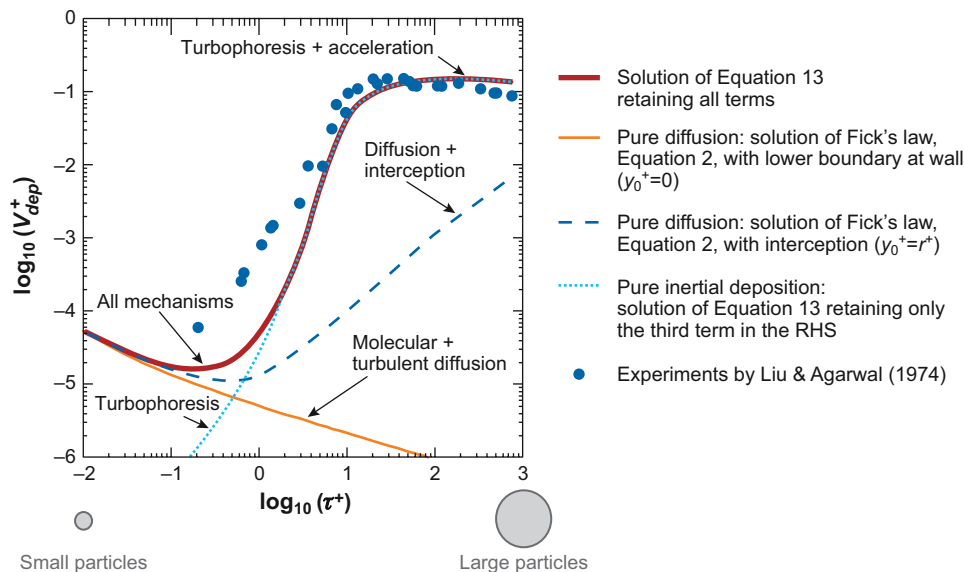
Figure 2

Computed deposition rate versus relaxation time (effects of pure diffusion, pure inertia, and interception): (*red line*) solution of Equation 13 retaining all terms; (*orange line*) pure diffusion, solution of Fick's law (Equation 2) with lower boundary at wall ($y_0^+ = 0$); (*dark blue dashed line*) pure diffusion, solution of Fick's law (Equation 2) with interception ($y_0^+ = r^+$); and (*light blue line*) pure inertial deposition, solution of Equation 13 retaining only the third term on the right-hand side (i.e., the convective flux term alone). Blue dots denote experiments by Liu & Agarwal (1974). For all computed curves, $k_s^+ = 0$, $\Delta T = 0$, and $\xi = 0$.

can be modeled without rebound); the pipe Reynolds number (Re_D) was 10,000; and $\rho_p^0/\rho_f = 770$. By combining u_* calculated from Blasius's formula, Guha (1997) has shown that $(D_B/\nu)^{2/3}\tau^{+1/3} = f(\mathrm{Re}_D, D, \rho_p^0/\rho, \text{fluid properties}) = \psi$. Thus for different values of ψ, different curves of V_{dep}^+ versus τ^+ are obtained.

    Figure 2 shows the relative importance of pure diffusion and pure inertial effects in the equation for mass flux (Equation 13). To isolate the effects of fluid turbulence, the flow considered is isothermal (no thermal diffusion), and all body forces (such as electrical forces) are absent. The pure diffusion case is calculated by assuming that the turbulence is homogeneous. The source term on the right-hand side of Equation 15c is zero; consequently, the convective velocity, $\bar{V}_{py}^c$, is zero. Under these circumstances, Equation 13 becomes identical to Equation 2—Fick's law of diffusion. The deposition velocity monotonically decreases with increasing relaxation time. This case was calculated by taking the lower boundary at $y^+ = 0$. The behavior of the deposition velocity, however, changes if one includes the effects of interception. The lower boundary is now given by Equation 20. As the lower boundary is shifted, the effective resistance against mass transfer decreases. For large relaxation times, this effect can more than offset the effect of the lower Brownian diffusion coefficient, D_B. For large relaxation times, the calculated deposition velocity therefore increases

substantially with increasing relaxation time owing to interception, even when the convective velocity, $\bar{V}_{py}^c$, is neglected. (The interception effect shown in **Figure 2** is the minimum because it is shown for $k_s = 0$, i.e., $b = 0$ in Equation 20.)

For calculating pure inertial effects, only the third term on the right-hand side of Equation 13 is retained. **Figure 2** shows that the convective velocity goes to zero for very small particles. Its effect on the deposition velocity has become comparable to that of pure diffusion around $\tau^+ \sim 0.2$. It then rises steeply by several orders of magnitude as τ^+ increases. The total deposition is calculated by retaining all terms in Equation 13. It merges with the pure diffusion case for very small particles and with the pure inertial case for large particles. One can clearly see the relative importance of diffusion, inertia, and interception in **Figure 2**.

Figure 3 shows the variation in deposition velocity with relaxation time for four different roughness parameters. The calculations show that the presence of a small amount of surface roughness even in the hydraulically smooth regime significantly enhances deposition, especially that of small particles. Given that the deposition velocity varies by more than four orders of magnitude in the range of investigation, it is remarkable that a simple, universal equation (Equation 13) agrees so well with measurements.

Figure 4 shows the effects of temperature gradient on the deposition velocity. (Equation 14 shows that the thermal drift has a stressphoretic and a thermophoretic component.) Even a small temperature difference (e.g., $\Delta T = 5$ K) has a significant effect on the deposition velocity, particularly for small particles. Considering that a modern gas turbine blade may be cooled by several hundred degrees Kelvin compared to the gas temperature, it is expected that thermophoresis plays an important

Figure 3

The effects of surface roughness on the predicted deposition rate. Equations 13 and 15c are solved for isothermal flow (no diffusion due to temperature gradient) for four values of the effective height of roughness elements k_s^+. Blue dots denote experiments by Liu & Agarwal (1974). For all computed curves, $\Delta T = 0, \xi = 0$, and there is no lift force.
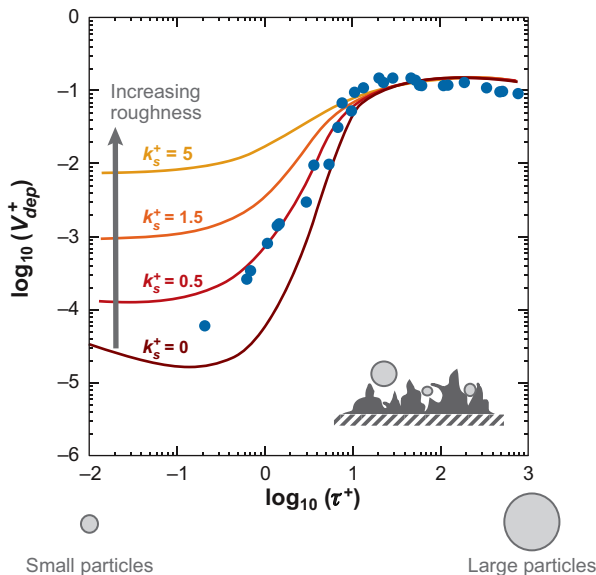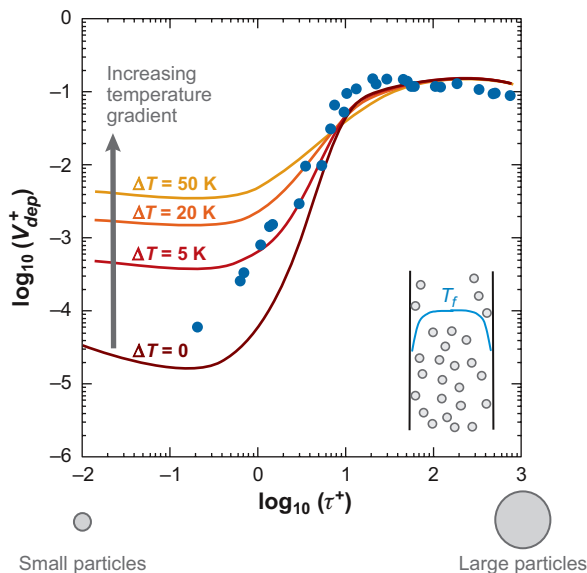
Effects of thermal diffusion on the predicted deposition rate. Equations 13 and 15c are solved for four values of ΔT, where ΔT is the temperature difference between the upper boundary of the calculation domain ($y^+ = 200$) and the pipe wall (the wall is cooled). Blue dots denote experiments by Liu & Agarwal (1974). For all computed curves, $k_s^+ = 0$, $\xi = 0$, and there is no lift force.

role there. For $1 < \tau^+ < 10$, there is an interaction between thermophoresis and turbophoresis.

Figure 5 shows that the electrical force due to mirror charging also has a significant effect on the deposition velocity. A parametric study on the amount of charge on each particle was conducted by specifying various values ξ (see Section 3.6). Interestingly, the most significant enhancement in deposition velocity takes place approximately
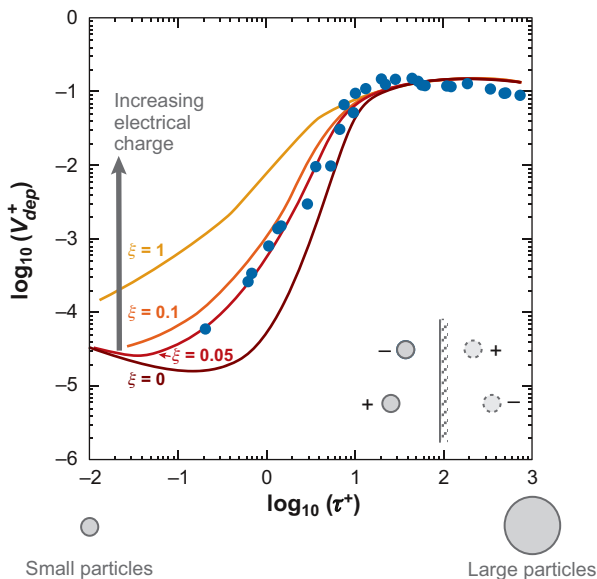
Effects of electrostatic charges (mirror charging) on the predicted deposition rate. Equations 13 and 15c are solved for four values of the parameter ξ, where ξ denotes the amount of electrical charge on each particle. Blue dots denote experiments by Liu & Agarwal (1974). For all computed curves, $k_s^+ = 0$, $\Delta T = 0$, and there is no lift force.

around $\tau^+ \sim 0.3$, at which the unassisted deposition curve begins to rise in **Figure 2**. Of course, the effects of the electrostatic forces are more prominent in the presence of an external electric field.

The particle transport given by Equation 13 has a diffusive and a convective part. The particles are transported by these two mechanisms. (The old free flight is effectively calculated by the present model of turbophoresis.) Very small particles complete the last part of their journey to the wall mainly by Brownian diffusion, and very large particles reach the wall mainly by the convective velocity imparted by turbophoresis. For intermediate-sized particles, a combination of both mechanisms is responsible.

In the region close to the wall (e.g., $y^+ < 20$), $\partial J/\partial y = 0$ for fully developed flow; the total particle flux (convective plus diffusive) remains constant (i.e., whatever particle flux enters into this region must reach the wall surface to satisfy continuity and to attain a steady state). Large particles may acquire sufficient $\bar{V}_{py}^c$ to enable them to coast to the surface—in this case, $\bar{\rho}_p$ would remain approximately constant close to the wall. The convective velocity may not be sufficient for small particles to coast all the way to the surface; to keep the total particle flux constant to satisfy continuity, the convective flux in this case may need to be supplemented by a large diffusive flux, which is achieved by the appropriate development of a particle density profile close to the wall. If the predicted value of $\bar{V}_{py}^c$ close to wall is inaccurate or the wall boundary condition for $\bar{\rho}_p$ is improper, then to keep J invariant close to the wall, the predicted concentration profile close to the wall would not be accurate.

7. DEPOSITION IN THE RESPIRATORY TRACT

An adult human breathes in 10,000 to 20,000 liters of air per day. The air brings with it a large quantity of particulate matter—micro-organisms, dusts, smokes, allergens, and other toxic or nontoxic aerosols—that may get deposited during the inhalation and exhalation process. The term total deposition refers to the collection of particles in the whole respiratory tract, and regional deposition is that in a specified region. The deposited particles may cause various effects, including many diseases. Sometimes particles of a known amount and size may also be deliberately introduced through the respiratory tract for therapeutic use (drug delivery), or for measurements of prophylactic and therapeutic effects of inhaled substances and pulmonary function, for example. The lung has a very large surface area; thus it is suitable for the delivery of drugs for both topical (minimizing side effects) and systemic (utilizing rapid access to the blood stream) purposes. For all these reasons, experimental determination and theoretical prediction of total and regional depositions are necessary. Consequently a large body of literature has grown on this subject. In this section, I present a synopsis of the principal ideas and the physical processes involved in respiratory tract deposition.

The flow in the upper part of the respiratory tract may be turbulent, whereas that in the lower tract is laminar. For the types of bifurcating airways, the critical Reynolds number above which flow becomes turbulent is lower than it is in a straight pipe. If the volume flow rate increases (e.g., during exercise), turbulent flow persists lower down

the tract than that during normal breathing. Turbulent flow increases deposition. In general, inertial impaction is significant in upper airways in which velocities are high; gravitational settling and Brownian diffusion are significant in lower airways in which residence times are longer. Typically, only a small proportion of the residual air in the alveolar region is actively replaced, leaving molecular diffusion to achieve a second stage of ventilation of the relatively stagnant residual air deep in the lung.

The deposition pattern of inhaled particles is strongly determined by the size of particles. The size range of natural and manmade particles can be large: For example, occupational dusts may be 0.001–1000 μm, pollen particles are 20–60 μm, consumer aerosol products are 2–6 μm, most cigarette smoke particles are 0.2–0.6 μm, and viruses and proteins may be in the range 0.001–0.05 μm. Part of the previously deposited particles may be removed by various clearance mechanisms, such as solubilization and absorption, coughing, sneezing, mucociliary transport, and alveolar clearance mechanisms involving pulmonary macrophages and other mechanisms (Brain & Valberg 1979). For a simple description, Heyder et al. (1986) presents deposition data in three regions: extrathoracic (nasal plus laryngeal), tracheobronchial (upper plus lower), and alveolar.

Deposition depends on the characteristics of the particles (size, shape, density, charge), morphology of the respiratory tract, and the breathing pattern (which determines the volumetric flow rate and the mean residence time of a particle). Heyder et al. (1986) and Stahlhofen (1980), among others, have given detailed experimental data. **Figure 6** shows a typical plot of fractional deposition in the three regions as a function of particle diameter (of unit density 1 g cm^{-3}); the main interest here is to explain the qualitative physics.
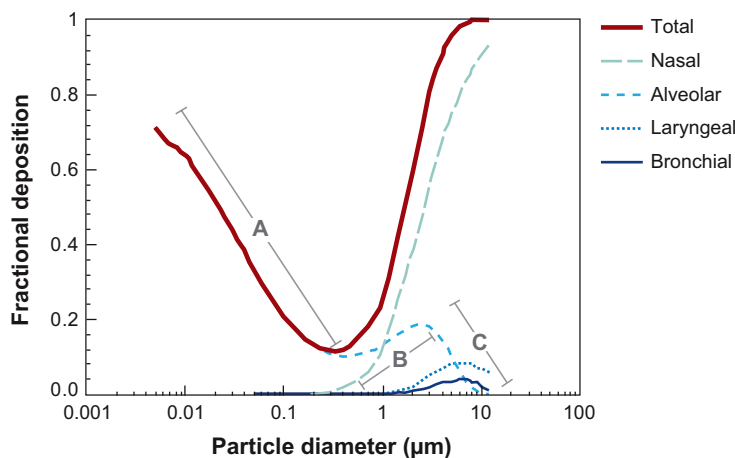

Figure 6

A typical regional deposition behavior in the human respiratory tract (as fractions of the total inhaled quantity). For particle sizes approximately less than 0.3 μm, the total deposition curve is almost superposed with the alveolar deposition curve. The alveolar deposition curve is divided into three segments A, B, and C to provide physical explanations regarding such variations. Data taken from Heyder et al. 1986.
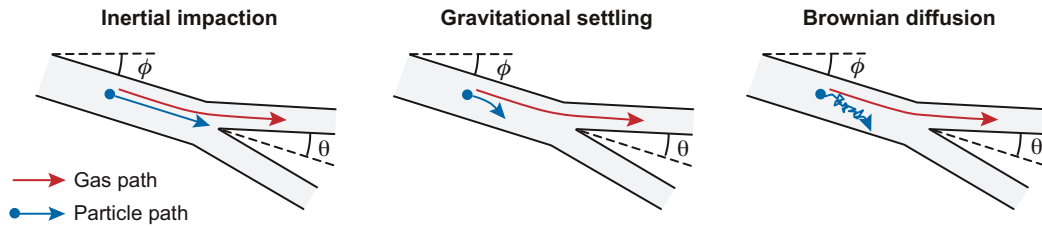
Inertial impaction   **Gravitational settling**   **Brownian diffusion**

→ Gas path
●→ Particle path

Figure 7

Three important mechanisms of deposition in the human respiratory tract.

There are three main mechanisms of deposition in the respiratory tract: inertial impaction, gravitational settling, and diffusion (schematically shown in **Figure 7**). Deposition due to both inertial impaction and gravitational settling increases with particle diameter, density of particulate material, flow rate, and duration of inspiration. Deposition due to Brownian diffusion decreases with particle diameter, increases with duration of inspiration, and does not depend on the density of particulate material or the flow rate.

The passages of the extrathoracic or nasopharyngeal section (from nostrils to larynx) are complex, with sharp bends, nasal hairs, and narrow cross sections (which results in high velocity), and the air flow is usually turbulent. Thus inertial impaction is the dominant mechanism. As a result of the relaxation time increasing with particle size, the deposition due to inertial impaction also increases with particle size. **Figure 6** shows this qualitative behavior in the nasal region. For (unit density) particle diameter in the range 1–10 μm, the majority of particles are deposited in the nasal passage; for a particle diameter greater than 10 μm, virtually all particles are removed from the flow by deposition in the nasal region.

Figure 6 shows that the deposition curves for both the laryngeal and bronchial regions exhibit the existence of a maxima. The collection efficiency of these regions, in fact, continuously improves with increasing particle diameter. However, the deposition in these regions as a fraction of the total inhaled quantity decreases above certain particle sizes because a greatly reduced number of those particles arrives at the inlet of these regions as a result of increased removal in the previous upstream regions.

The deposition curve in the alveolar region shows three segments (**Figure 6**). In segment A, the particles are so small that Brownian diffusion dominates; the Brownian diffusion coefficient decreases with increasing particle diameter; hence the deposition decreases with increasing particle size. In segment B, gravitational settling has become the dominant mechanism; hence the deposition increases with increasing particle size. However, after a certain particle size (i.e., in segment C), the fractional deposition decreases as a result of the increased removal of particles (owing to inertial impaction and gravitational settling) in the previous upstream regions of the respiratory tract.

Figure 6 depicts the fundamental processes for nasal breathing. Experimental data for oral breathing are given by, for example, Heyder et al. (1986). Total deposition is higher for nasal breathing as compared to oral breathing, since the nasal passages

are very effective collectors, particularly of large particles. However, the laryngeal, bronchial, and alveolar depositions are lower for nasal breathing.

Theories (e.g., Beeckmans 1965, Landahl 1963, Taulbee & Yu 1975) and semiempirical methods (e.g., Heyder et al. 1986, Int. Comm. Respir. Prot. 1994) have been developed for the prediction of deposition in the respiratory tract. In recent years the application of CFD has opened up the possibility of achieving theoretical solutions for realistic, complex flow passages. Mostly, commercially available CFD software packages have been used for the numerical simulation of the air flow field in the nasopharyngeal or tracheobronchial tree. Particle deposition is then calculated mostly by nonstochastic Lagrangian particle tracking (thus excluding any effect of fluid turbulence on particle motion) and occasionally by Eulerian modeling (but excluding turbophoresis). It will be interesting to study any effects of turbophoresis on the deposition in the upper airways. There is no doubt that computational studies of deposition in the respiratory tract will grow vigorously in the future. Once validated by experiments, the CFD tools have the potential to significantly enhance our understanding for cases in which direct measurements would be difficult.

8. DEPOSITION IN GAS AND STEAM TURBINES

Both gas and steam turbine blades experience the high-speed flow of a gas or a vapor through highly curved, complex three-dimensional flow passages. Any suspended solid particles or liquid droplets therefore can move and get deposited by inertial impaction (owing to streamline curvature) and by molecular and turbulent transport processes as explained above. In cooled gas turbines, in which the blade may be 300–400 K cooler than the gas, the thermal gradient also strongly influences the motion of particles [in the appropriate size range (**Figure 4**)]. The flow through turbine blades therefore provides a good opportunity to test theoretical predictions. The flow field in the primary gas (or vapor) is determined by Eulerian flow solvers (e.g., Denton & Dawes 1999, Mei & Guha 2005); therefore, it is most profitable to integrate the unified Eulerian advection-diffusion model of deposition explained in Section 5.2 with any available single-phase flow solver. The particle equations given by Guha (1997) can be used for developing boundary layers.

In low-pressure steam turbines, droplets form owing to homogeneous nucleation and then grow rapidly (Guha 1995, 1998b; Guha & Young 1994; Gyarmathy 1962). Experiments show that the water in turbines exists in two quite different forms. Usually more than 90% of the mass is concentrated in the fog, which consists of a very large number of very fine droplets (diameter 0.05–2.0 μm). The rest is in the form of coarse droplets that are much larger (diameter 20–200 μm). Coarse water is formed as a small proportion of the fog (typically 2%–4% per blade row) is deposited on the blade surface (Crane 1973, Parker & Ryley 1969/1970, Young & Yau 1988). The deposited water is drawn toward the trailing edge by the steam flow (or centrifuged toward the casing on moving blades), at which it is re-entrained in the form of large droplets. Impingement of the large droplets causes blade erosion.

Menguturk & Sverdrup (1982) have computed deposition on gas turbine blades. Deposition causes erosion and corrosion. The turbines, situated downstream of the
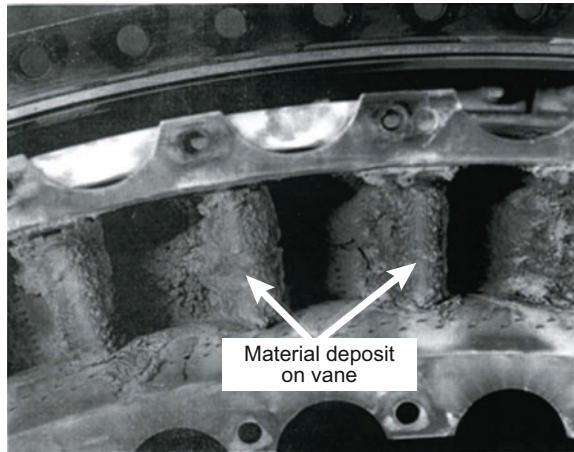
combustion chamber, face the flow of combustion products through them, resulting
in the deposition of particulate material. Prediction (and control) of deposition may
be even more important in future turbines working with alternative fuels, for example,
in directly coal-fired turbines. Wenglarz & Fox (1990) studied deposition from coal-
water fuels, Ragland et al. (1995) described ash deposition in a wood-fired gas turbine,
and Dunn et al. (1994) described experiments on the operation of gas turbines in
volcanic-ash clouds. **Figure 8** shows an example of the severe degradation of the
flow path that may result from deposition; not only are the aerodynamics and the
gas turbine operation as a whole seriously affected as a result of such a large amount
of deposition, but the deposited (and melted) material also blocks the cooling holes
of the turbine blades. An aircraft engine may experience such heavily particle-laden
flows owing to explosive volcanic eruptions, sand storm, and military conflicts, for
example. In a detailed study, Campbell (1990) reported that, in 17 years prior to the
study, there were numerous aircraft encounters with volcanic ash, 24 of which were
major incidents in which significant damage to the airplane or engines had occurred
[approximately 500 (explosive-type) volcanoes are active worldwide].

9. CONCLUDING COMMENTS

The above sections discuss theories of deposition with two example applications;
similar principles are valid for fluid-particle flows encountered in other fields. Appli-
cations of CFD will dominate future research and engineering calculations of depo-
sition, as there is scope for careful experiments for the development and validation
of theoretical predictions. In the past, Lagrangian tracking methods have commonly
been applied for the calculation of deposition in complex geometries. The recently
developed unified advection-diffusion method (Section 5.2) now offers the prospect
of a Eulerian solution in similar situations. Both Lagrangian and Eulerian methods
have their strengths and challenges, and each can help in the further refinement of
the other.

DISCLOSURE STATEMENT

The author is not aware of any biases that might be perceived as affecting the objectivity of this review.

ACKNOWLEDGEMENTS

LITERATURE CITED

Beal SK. 1970. Deposition of particles in turbulent flow on channel or pipe walls. *Nucl. Sci. Eng.* 40:1–11

Becker E. 1970. Relaxation effects in gas dynamics. *Aeronaut. J.* 74:736–48

Beeckmans JM. 1965. Deposition of aerosols in respiratory tract. I. Mathematical analysis and comparison with experimental data. *Can. J. Physiol. Pharmacol.* 43:157–72

Berlemont A, Desjonqueres P, Gouesbet G. 1990. Particle Lagrangian simulation in turbulent flows. *Int. J. Multiph. Flow* 16:19–34

Binder JL, Hanratty TJ. 1991. A diffusion model for droplet deposition in gas/liquid annular flow. *Int. J. Multiph. Flow* 17:1–11

Borgas MS, Sawford BL. 1996. Molecular diffusion and viscous effects in grid turbulence. *J. Fluid Mech.* 324:25–54

Brain JD, Valberg PA. 1979. Deposition of aerosol in the respiratory tract. *Am. Rev. Respir. Dis.* 120:1325–73

Bremhorst K, Walker TB. 1973. Spectral measurements of turbulent momentum transfer in fully developed pipe flow. *J. Fluid Mech.* 61:173–86

Brooke JW, Hanratty TJ, McLaughlin JB. 1994. Free-flight mixing and deposition of aerosols. *Phys. Fluids* 6:3404–15

Campbell EE. 1990. Volcanic ash. *Proc. 747 Flight Oper. Symp. Seattle, WA, Oct. 9–11*, pp. 2.3.1–34. Seattle: Boeing Commer. Aircr. Co.

Caporaloni M, Tampieri F, Trombetti F, Vittori O. 1975. Transport of particles in nonisotropic air turbulence. *J. Atmos. Sci.* 32:565–68

Chapman DR, Kuhn GD. 1986. The limiting behaviour of turbulence near a wall. *J. Fluid Mech.* 170:265–92

Cleaver JW, Yates B. 1975. A sub-layer model for the deposition of particles from a turbulent flow. *Chem. Eng. Sci.* 30:983–92

Clift R, Grace JR, Weber ME. 1978. *Bubbles, Drops and Particles*. New York: Academic

Crane RI. 1973. Deposition of fog drops on low pressure steam turbine blades. *Int. J. Mech. Sci.* 15:613–31

Crowe CT. 1982. Review. Numerical models for dilute gas-particle flows. *J. Fluids Eng.* 104:297–303

Cunningham E. 1910. On the velocity of steady fall of spherical particles through fluid medium. *Proc. R. Soc. Lond. Ser. A* 83:357–65

Davies CN. 1945. Definitive equations for the fluid resistance of spheres. *Proc. Phys. Soc. Lond.* 57:259–70

Davies CN, ed. 1966. *Aerosol Science*. London: Academic

Denton JD, Dawes WN. 1999. Computational fluid dynamics for turbomachinery design. *Proc. Inst. Mech. Eng. C* 213:107–24

Dunn MG, Baran AJ, Miatech J. 1994. Operation of gas turbine engines in volcanic ash clouds. *ASME Tech. Pap. 94-GT-170*

Durbin PA. 1980. A random flight model of inhomogeneous turbulent dispersion. *Phys. Fluids* 23:2151–53

Fan F, Ahmadi G. 1993. A sublayer model for turbulent deposition of particles in vertical ducts with smooth and rough surfaces. *J. Aerosol Sci.* 24:45–64

Fernandez De La Mora JF, Rosner DE. 1982. Effects of inertia on the diffusional deposition of small particles to spheres and cylinders at low Reynolds numbers. *J. Fluid Mech.* 125:379–95

Fichman M, Gutfinger C, Pnueli D. 1988. A model for turbulent deposition of aerosols. *J. Aerosol Sci.* 19:123–36

Finnicum DS, Hanratty TJ. 1985. Turbulent normal velocity fluctuations close to a wall. *Phys. Fluids* 28:1654–58

Friedlander SK, Johnstone HF. 1957. Deposition of suspended particles from turbulent gas streams. *Ind. Eng. Chem.* 49:1151–56

Gosman AD, Ioannides E. 1983. Aspects of computer simulation of liquid-fueled combustors. *J. Energy* 7:482–90

Graham DI, James PW. 1996. Turbulent dispersion of particles using eddy interaction models. *Int. J. Multiph. Flow* 22:157–75

Granville PS. 1990. A near-wall eddy viscosity formula for turbulent boundary layers in pressure gradients suitable for momentum, heat, or mass transfer. *Trans. ASME J. Fluids Eng.* 112:240–43

Grass AJ. 1971. Structural features of turbulent flow over smooth and rough boundaries. *J. Fluid Mech.* 50:233–55

Guha A. 1994. A unified theory of aerodynamic and condensation shock waves in vapour-droplet flows with or without a carrier gas. *Phys. Fluids* 6:1893–913

Guha A. 1995. Two-phase flows with phase transition: nucleation, droplet growth and condensation in pure steam flows; fluid dynamics with interphase transport of mass, momentum and energy in pure vapour-droplet mixtures; application of the non-equilibrium theory to steam turbines. In *Two-Phase Flows with Phase Transition*, pp. 1–110. Von Karman Inst. Lect. Ser. 1995–06. Belgium: von Karman Inst. Fluid Dyn.

Guha A. 1997. A unified Eulerian theory of turbulent deposition to smooth and rough surfaces. *J. Aerosol Sci.* 28:1517–37

Guha A. 1998a. A unified theory for the interpretation of total pressure and temperature in two-phase flows at subsonic and supersonic speeds. *Proc. R. Soc. Ser. A* 454:671–95

Guha A. 1998b. Computation, analysis and theory of two-phase flows. *Aeronaut. J.* 102:71–82

Guha A. 2007. Shock waves in fluids with interphase transport of mass, momentum and energy (vapour-droplet mixtures and solid-particle-laden gases). In *Shock Waves Science and Technology Reference Library, Vol. 1, Multiphase Flows*, ed. MEH van Dongen, pp. 135–86. Berlin: Springer

Guha A, Young JB. 1991. Time-marching prediction of unsteady condensation phenomena due to supercritical heat addition. In *Turbomachinery: Latest Developments in a Changing Scene*, pp. 167–77. London: Inst. Mech. Eng.

Guha A, Young JB. 1994. The effect of flow unsteadiness on the homogeneous nucleation of water droplets in steam turbines. *Philos. Trans. R. Soc. Lond. A* 349:445–72

Gyarmathy G. 1962. Bases of a theory for wet steam turbines. *Bull. 6*, Inst. Therm. Turbomach., Fed. Tech. Univ., Zurich (CEGB translation 3017)

Hesketh HE. 1977. *Fine Particles in Gaseous Media*. Ann Arbor, MI: Ann Arbor Sci.

Heyder J, Gebhart J, Rudolf G, Schiller CF, Stahlhofen W. 1986. Deposition of particles in the human respiratory tract in the size range 0.005–15 μm. *J. Aerosol Sci.* 17:811–25

Hinds WC. 1999. *Aerosol Technology: Properties, Behaviour and Measurement of Airborne Particles*. New York: Wiley

Hutchinson P, Hewitt GF, Dukler AE. 1971. Deposition of liquid or solid dispersions from turbulent gas streams: a stochastic model. *Chem. Eng. Sci.* 26:419–39

Int. Comm. Respir. Prot. 1994. *Human Respiratory Tract Model for Radiological Protection*. Int. Comm. Respir. Prot. Publ. 66. Oxford: Pergamon

Johansen ST. 1991. The deposition of particles on vertical walls. *Int. J. Multiph. Flow* 17:355–76

Kallio GA, Reeks MW. 1989. A numerical simulation of particle deposition in turbulent boundary layers. *Int. J. Multiph. Flow* 15:433–46

Kay JM, Nedderman RM. 1988. *Fluid Mechanics and Transfer Processes*. Cambridge, UK: Cambridge Univ. Press

Kim J, Moin P, Moser R. 1987. Turbulence statistics in fully developed channel flow. *J. Fluid Mech.* 177:136–66

Kreplin HP, Eckelmann H. 1979. Behaviour of the three fluctuating velocity components in the wall region of a turbulent channel flow. *Phys. Fluids* 22:1233–39

Landahl HD. 1963. Particle removal by the respiratory system. *Bull. Math. Biophys.* 25:29–39

Laufer J. 1954. The structure of turbulence in fully developed pipe flow. *NACA Tech. Rep. 1174*

Liu BYH, Agarwal JK. 1974. Experimental observation of aerosol deposition in turbulent flow. *J. Aerosol Sci.* 5:145–55

Liu BYH, Ilori TY. 1974. Aerosol deposition in turbulent pipe flow. *Environ. Sci. Technol.* 8:351–56

Luhar AK, Britter RE. 1989. A random walk model for dispersion in inhomogeneous turbulence in a convective boundary layer. *Atmos. Environ.* 23:1911–24

Marchioli C, Soldati A. 2002. Mechanisms for particle transfer and segregation in turbulent boundary layers. *J. Fluid Mech.* 468:283–315

Maxey MR, Riley JJ. 1983. Equation of motion for a small rigid sphere in a nonuniform flow. *Phys. Fluids* 26:883–89

McCoy DD, Hanratty TJ. 1977. Rate of deposition of droplets in annular two-phase flow. *Int. J. Multiph. Flow* 3:319–31

Mei Y, Guha A. 2005. Implicit numerical simulation of transonic flow through turbine cascades on unstructured grids. *Proc. Inst. Mech. Eng. A J. Power Energy* 219(A1):35–47

Menguturk M, Sverdrup EF. 1982. A theory for fine particle deposition in two-dimensional boundary layer flows and application to gas turbines. *J. Eng. Power* 104:69–76

Monin AS, Yaglom AM. 1975. *Statistical Fluid Mechanics: Mechanics of Turbulence*, Vol. 2. Cambridge, MA: MIT Press

Morsi SA, Alexander AJ. 1972. An investigation of particle trajectories in two-phase flow systems. *J. Fluid Mech.* 55:193–208

Nadler B, Hollerbach U, Eisenberg RS. 2003. Dielectric boundary force and its crucial role in gramicidin. *Phys. Rev. E* 68:021905

Ounis H, Ahmadi G, McLaughlin JB. 1993. Brownian particle deposition in a directly simulated turbulent channel flow. *Phys. Fluids* 5:1427–32

Papavergos PG, Hedley AB. 1984. Particle deposition behaviour from turbulent flows. *Chem. Eng. Res. Des.* 62:275–95

Parker GJ, Ryley DJ. 1969/1970. Equipment and techniques for studying the deposition of submicron particles on turbine blades. *Proc. Inst. Mech. Eng.* 184(3C):43–51

Pismen LM, Nir A. 1978. On the motion of suspended particles in stationary homogeneous turbulence. *J. Fluid Mech.* 84:193–206

Ragland KW, Misra MK, Aerts DJ, Palmer CA. 1995. Ash deposition in a wood-fired gas turbine. *J. Eng. Gas Turbines Power* 117:509–12

Ramshaw JD. 1979. Brownian motion in a flowing fluid. *Phys. Fluids* 22:1595–601

Reeks MW. 1977. On the dispersion of small particles suspended in an isotropic turbulent fluid. *J. Fluid Mech.* 83:529–46

Reeks MW. 1983. The transport of discrete particles in inhomogeneous turbulence. *J. Aerosol Sci.* 14:729–39

Reeks MW. 1991. On a kinetic equation for the transport of particles in turbulent flows. *Phys. Fluids A* 3:446–56

Reeks MW. 1992. On the continuum equations for dispersed particles in nonuniform flows. *Phys. Fluids* 4:1290–303

Reeks MW, Skyrme G. 1976. The dependence of particle deposition velocity on particle inertia in turbulent pipe flow. *J. Aerosol Sci.* 7:485–95

Rizk MA, Elghobashi SE. 1985. The motion of a spherical particle suspended in a turbulent flow near a plane wall. *Phys. Fluids* 28:806–17

Saffman PG. 1965. The lift on a small sphere in a slow shear flow. *J. Fluid Mech.* 22:385–400

Saffman PG. 1968. Corrigendum to "the lift on a small sphere in a slow shear flow." *J. Fluid Mech.* 31:624

Sawford BL. 1982. Lagrangian Monte Carlo simulation of turbulent motion of a pair of particles. *Q. J. R. Meteorol. Soc.* 108:207–13

Shin M, Lee JW. 2001. Memory effect in the Eulerian particle deposition in a fully developed turbulent channel flow. *J. Aerosol Sci.* 32:675–93

Shuen JS, Chen LD, Faeth GM. 1983. Evaluation of a stochastic model of particle dispersion in a turbulent round jet. *Chem. Eng. J.* 29:167–70

Simonin O, Deutsch E, Minier M. 1993. Eulerian prediction of the fluid-particle correlated motion in turbulent two-phase flows. *Appl. Sci. Res.* 51:275–83

Soo SL. 1990. *Multiphase Fluid Dynamics*. Beijing: Science

Stahlhofen W. 1980. Experimental determination of the regional deposition of aerosol particles in the human respiratory tract. *Am. Ind. Hyg. Assoc. J.* 41:385–98

Talbot L, Cheng RK, Schefer RW, Willis DR. 1980. Thermophoresis of particles in a heated boundary layer. *J. Fluid Mech.* 101:737–58

Taulbee DB, Yu CP. 1975. Theory of aerosol deposition in human respiratory tract. *J. Appl. Physiol.* 38:77–85

Thomson DJ. 1987. Criteria for the selection of stochastic models of particle trajectories in turbulent flows. *J. Fluid Mech.* 180:529–56

Vames JS, Hanratty TJ. 1988. Turbulent dispersion of droplets for air flow in a pipe. *Exp. Fluids* 6:94–104

Walklate PJ. 1987. A random-walk model for dispersion of heavy particles in turbulent air flow. *Bound. Layer Meteorol.* 39:175–90

Wang LP, Stock DE. 1992. Stochastic trajectory models for turbulent diffusion: Monte Carlo process versus Markov chains. *Atmos. Environ.* 26:A1599–607

Wang Q, Squires KD. 1996. Large eddy simulation of particle-laden turbulent channel flow. *Phys. Fluids* 8:1207–23

Wells AC, Chamberlain AC. 1967. Transport of small particles to vertical surfaces. *Br. J. Appl. Phys.* 18:1793–99

Wenglarz RA, Fox RG. 1990. Physical aspects of deposition from coal-water fuels under gas turbine conditions. *J. Eng. Gas Turbines Power* 112:9–14

Wood NB. 1981. A simple method for the calculation of turbulent deposition to smooth and rough surfaces. *J. Aerosol Sci.* 12:275–90

Young J, Leeming A. 1997. A theory of particle deposition in turbulent pipe flow. *J. Fluid Mech.* 340:129–59

Young JB, Yau KK. 1988. The inertial deposition of fog droplets on steam turbine blades. *J. Turbomach.* 110:155–62

Zaichik LI. 1999. A statistical model of particle transport and heat transfer in turbulent shear flows. *Phys. Fluids* 11:1521–34

Contents

Indexes

Errata

An online log of corrections to *Annual Review of Fluid Mechanics* articles may be
found at http://fluid.annualreviews.org/errata.shtml